Aeroacoustics taking Fluid-Structure Interaction into Account

M. Kaltenbacher[1] and S. Becker[2] and J. Grabinger[3] and F. Schäfer[4]

[1] *Chair of Applied Mechatronics, University of Klagenfurt, Austria, Email: manfred.kaltenbacher@uni-klu.ac.at*

[2] *Institute of Fluid Mechanics, University of Erlangen, Germany, Email: stefan.becker@lstm.uni-erlangen.de*

[3] *Chair of Sensor Technology, University of Erlangen, Germany, Email: jens.grabinger@lse.eei.uni-erlangen.de*

[4] *Institute of Fluid Mechanics, University of Erlangen, Germany, Email: frank.schaefer@lstm.uni-erlangen.de*

Introduction

In the last years, manufacturers have started to consider the aerodynamic noise level in many industrial applications as a relevant design parameter (e.g. airplanes, cars, air conditioning systems, etc.). Because of the growing demand for reducing noise levels and for fulfilling noise regulations, there is a great motivation to investigate the basic aeroacoustic phenomena and mechanisms of sound generation and propagation.

In the present work, we investigate the three field coupling for a flow past a thin flexible structure. Our developed numerical algorithms are capable to simulate the complex interaction between fluid, structure and acoustics. The scheme is based on a partitioned approach employing a finite-volume flow solver and a finite-element structural mechanics and acoustics solver. An important feature of the computational scheme is that it allows for a separate prediction of flow-induced and vibrational sound. We will present detailed numerical studies of the interaction of the fluid flow with the flexible structure and the generated noise. Moreover, a comparison of computational results to our experimental investigations will be provided.

Numerical Scheme

A partitioned computation scheme is used for the simulation of the fluid-structure-acoustic interaction of the present test case. Two different simulation codes are employed. The numerical flow computation is carried out with FASTEST-3D [1], a finite-volume CFD solver developed at the Institute of Fluid Mechanics, University of Erlangen-Nuremberg. For the structural mechanics and the acoustic computations the finite-element multiphysics solver CFS++ [2] is applied, which has been developed at the Chair of Sensor Technology, University of Erlangen-Nuremberg and Chair of Applied Mechatronics, University of Klagenfurt.

In the present computational scheme, the effect of the acoustics on the structure as well as the fluid is neglected since the expected acoustic pressure fluctuations are much smaller than the overall fluid pressure. Therefore, the fluid-structure-acoustic interaction can be split into three parts which are treated independently: fluid-structure interaction, fluid-acoustic coupling and structure-acoustic coupling (see Figure 1). A detailed description of the resulting computational scheme can be found in [3]. For fluid-structure interaction an implicit coupling between FASTEST-3D and CFS++ is applied. The exchange of data between the finite-volume and the finite-element discretization is realized by MpCCI [4]. The acoustic computations are performed with CFS++ using a finite-element discretization of Lighthill's wave equation, which has been extended to also take mechanical - acoustic coupling into account (vibrational sound) [5].

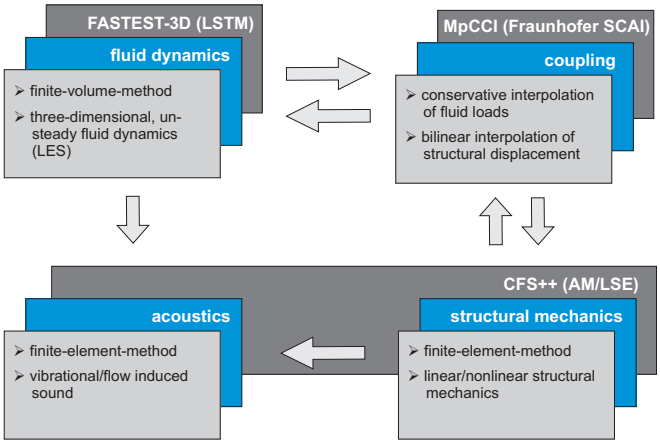

Figure 1: Scheme for the code-coupling and data exchange.

Test Case

The basic setup of the test case considered in the present work consists of a flexible plate-like structure which is part of an otherwise rigid wall. In order to study the influence of geometric flow disturbances on the resulting acoustic field, two different configurations have been investigated: one case with a square cylinder obstacle in front of the flexible plate as shown in Figure 2(a), and a second case without obstacle displayed in Figure 2(b). In the remainder of the paper, the two configurations are referred to as case A and B, respectively.

A flow of air at ambient conditions is considered. The free-stream velocity U_∞ is set to 20 m/s. The plate is made of stainless steel with a thickness of 40 μm (density $\rho_s = 7\,850$ kg/m^3, modulus of elasticity $E = 2 \cdot 10^{11}$ kg/ms^2, Poisson number $\nu = 0.3$, pre-stressing in streamwise direction $7 \cdot 10^6$ N/m^2). In case A, the edge length of the square cylinder is $D = 0.02$ m. The streamwise extension of the flexible plate amounts to $7.5\,D$ in both configurations. Because of the pre-stressing the plate is clamped over a length of $0.5\,D$ at the upstream and the downstream edge, respectively.

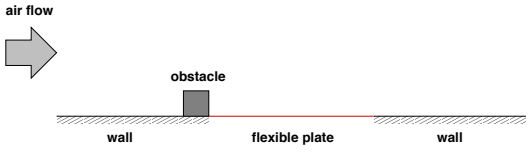

(a) Case A

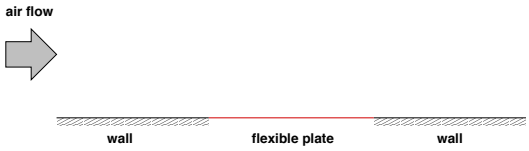

(b) Case B

Figure 2: Setup of the test case.

The flow simulation is carried out by solving the incompressible Navier-Stokes equations with discretizations of second order accuracy in both space and time. The considered flow domain for configuration A is depicted in Figure 3(a). Basically, the same setup is used for configuration B, but without obstacle. The computations are performed as large-eddy simulations (LES) with the Smagorinsky model and an implicit time discretization scheme. Since all boundary layers have to be resolved properly, block-structured meshes with up to 8 million control volumes are used for the spatial discretization of the flow domain.

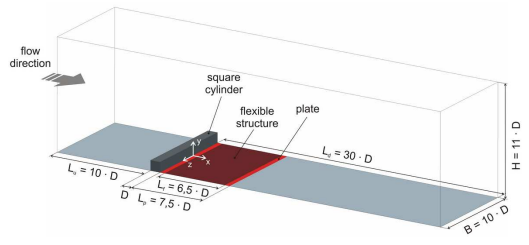

(a) Flow domain

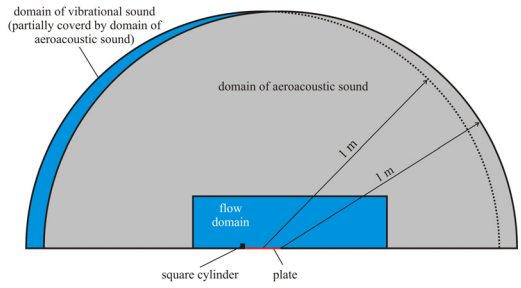

(b) Acoustics domains

Figure 3: Computational domains for case A.

For the structural mechanics computation the flexible plate is discretized using 13 000 hexahedron elements. Bilinear basis functions with an incompatible mode approach to account for shear locking effects are applied together with an implicit second order time discretization scheme of the Newmark type [6]. In accordance with the specification of the test case, the flexible plate is prestressed in the streamwise direction.

The computational domain for acoustics is quite larger than for the flow, since we are interested in the radiation of noise to the far field. A schematic is shown in Figure 3(b). Up to 420 000 bilinear elements are used for the spatial discretization of the acoustic domains. Absorbing boundary conditions are applied at the top boundary in order to guarantee for free radiation conditions.

Results

Flexible plate with square cylinder

A comparison of the averaged velocity field obtained by simulation and Laser-Doppler Anemometry (LDA) measurements, respectively, is provided in Figure 4. The most dominant flow structure is a large region of recirculation which is located behind the square cylinder. There is only a minor difference in the recirculation length, which is measured somewhat shorter in the experiments than in the computations.

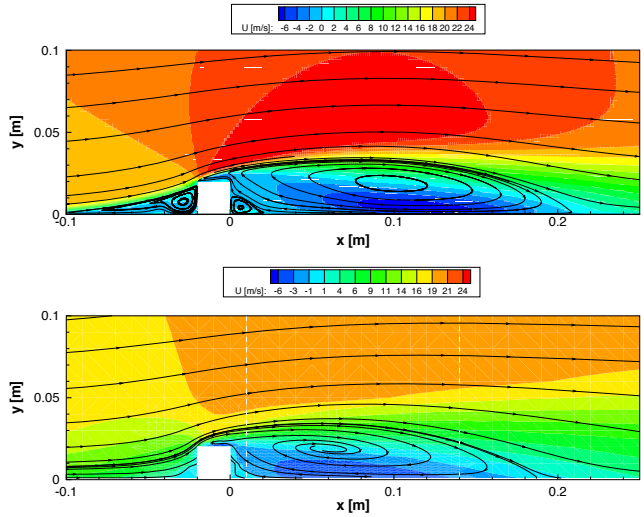

Figure 4: Average velocity in main flow direction for case A: simulation (top) and experiment (bottom).

The computed displacement amplitudes of the flexible plate due to fluid-structure interaction are in the range of 2 mm. The frequency spectra of the plate vibrations and its velocity in normal direction are shown in Figure 5. Besides the first eigenfrequency, also higher oscillation modes are excited which are very close to the odd eigenfrequencies of the flexible plate.

The resulting flow induced sound based on Lighthill's analogy is shown in Figure 6. The frequency spectra of the sound exhibit a broadband character with a peak between 100 and 200 Hz, which we relate to the influence of the plate vibration on the flow induced sound. The frequency spectra of the computed vibrational sound pressure level are plotted in Figure 7. A dominant peak at 140 Hz can be found, which corresponds well with the first eigenfrequency of the plate. Furthermore, higher-frequency peaks can be found, which are related to the higher oscillation modes of the plate. This is in very good accordance with the spectra of the plate oscillation presented in Figure 5.

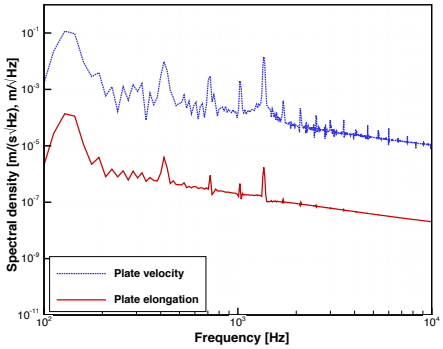

Figure 5: Frequency spectra of the plate vibration and velocity at a point in the center of the plate (case A).

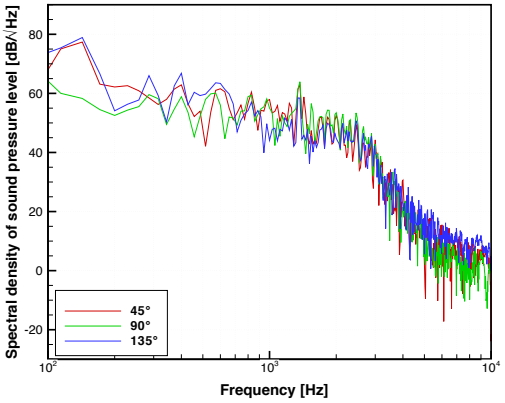

Figure 6: Computed frequency spectra at 45, 90 and 135 degree of the flow induced sound in a distance of 1 m from the downstream edge of the plate (case A).

Flexible plate without obstacle

The computed displacement amplitudes of the flexible plate without square cylinder are just in the range of 0.2 mm. This indicates that the excitation of the plate by the turbulent boundary layer in case B is much weaker than by the flow in the wake of the square cylinder in case A. The frequency spectra of the plate vibration and its velocity in normal direction are plotted in Figure 8. Compared to case A, the frequency of the most dominant mode is shifted towards 120 Hz which is significantly less than the first eigenfrequency of the plate at 142 Hz.

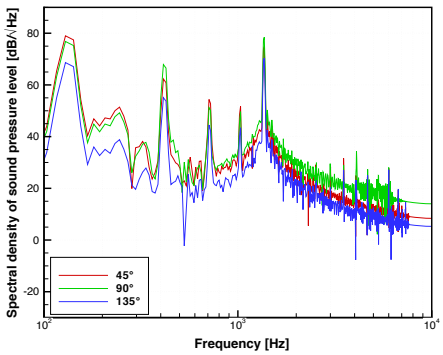

Figure 7: Computed vibrational sound in a distance of 1 m from the center of the plate (case A).

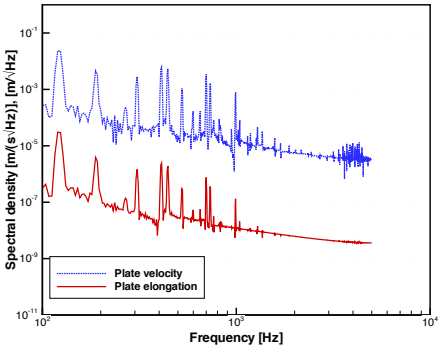

Figure 8: Frequency spectra of the plate vibration and velocity at a point in the center of the plate (case B).

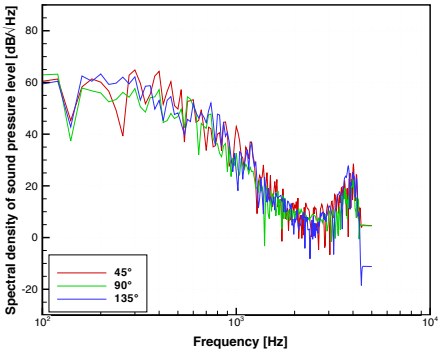

Figure 9: Computed frequency spectra at 45, 90 and 135 degree of flow induced sound in a distance of 1 m from the downstream edge of the plate (case B).

The computed flow induced sound is displayed in Figure 9. A broadband frequency spectrum can be observed with no significant peak in the vicinity of the plate's major oscillation frequency. Flow induced sound and plate vibration seem to be fully decoupled, while in case A a slight influence of the plate vibration was found. This might be attributed to the smaller vibration amplitude in case B, which certainly leads to a smaller influence of the vibration on the flow field. Apart from the peak between 100 and 200 Hz in case A, below 400 Hz the computed sound pressure level is of the same order of magnitude in both cases A and B. Above 400 Hz, a stronger decrease is seen for the case without obstacle. The computed vibrational sound is plotted in Figure 10. It is found that the amplitudes of the most prominent peaks are lower than in case A.

Comparison to experimental data

Frequency spectra of the measured sound pressure level are plotted in Figure 11. These include spectra obtained for the empty test section, for the flexible plate without square cylinder (case B) and for the flexible plate with square cylinder (case A). In comparison to the empty test section, the case of the flexible plate without obstacle shows several peaks in the range between 100 and 200 Hz, which corresponds approximately to the first eigenfrequency of the plate. For higher frequencies, there is only a small difference to the reference case with the empty test section. The presence of the square

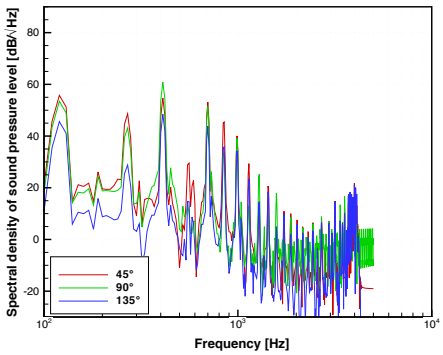

Figure 10: Computed vibrational sound in a distance of 1 m from the center of the plate (case B).

cylinder obstacle leads to a significant increase in sound pressure level in the range between 100 and 200 Hz, with a dominant peak at about 115 Hz. Additionally, at higher frequencies a large increase in broadband noise is observed, which is in accordance to the simulation results (see Figure 6).

Comparing the frequency spectra of the computed sound pressure level with the experimental findings in Figure 11, despite of quantitative differences it can be noticed that the overall tendency in the experiment is well reflected by the simulation. In both experiment and simulation the flow disturbance caused by the square cylinder leads to a significant increase in sound pressure level compared to the case without obstacle. In this respect, the tonal component observed between 100 and 200 Hz in the measurements corresponds well to the computed vibrational sound due to the first eigenmode of the plate.

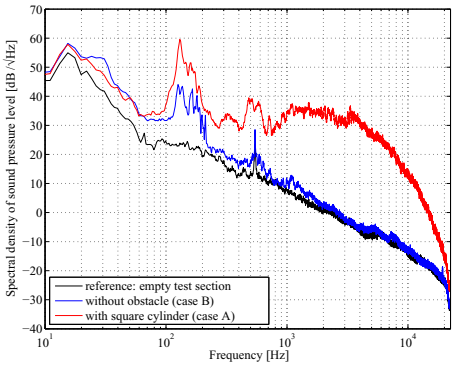

Figure 11: Measured sound pressure level

Conclusion

Numerical investigations of the noise generated by the flow over a thin flexible plate were presented. Two different configurations were considered: one case with a square cylinder obstacle located in front of the flexible plate, and one case without obstacle. The applied computational scheme allowed for a separate determination of flow induced and vibrational sound, which is generally very difficult to achieve experimentally.

The overall tendency of the computed sound pressure levels was in accordance with our experimental data.

Acknowledgments

Financial Support by the Bavarian Research Foundation is gratefully acknowledged.

References

[1] Durst, F. & Schäfer, M.: *A Parallel Block-Structured Multigrid Method for the Prediction of Incompressible Flows.* International Journal of Numerical Methods Fluids, vol. 22, pp. 549–565, 1996.

[2] Kaltenbacher, M., Hauck, A., Triebenbacher, S., Link, G. & Bahr, L.: *CFS++: Coupled Field Simulation.* 2007.

[3] Schäfer, F., Kniesburges, S., Uffinger, T., Becker, S., Grabinger, J., Link, G. & Kaltenbacher, M.: *Numerical Simulation of Fluid-Structure- and Fluid-Structure-Acoustic Interaction based on a Partitioned Coupling Scheme.* In *High Performance Computing in Science and Engineering, Munich 2007*, Springer, 2008 (to appear).

[4] Ahrem, R., Hackenberg, M. G., Redler, R. & Roggenbunck, J.: *MpCCI Mesh Based Parallel Code Coupling Interface.* Institute of Algorithms and Scientific Computing (SCAI), GMD, `http://www.mpcci.org/`, 2003.

[5] Kaltenbacher, M., Escobar, M., Becker, S. & Ali, I.: *Computational Aeroacoustics based on Lighthill's Analogy.* In *Computational Acoustics of Noise Propagation in Fluids*, pp. 115–142, Springer, 2008.

[6] Kaltenbacher, M.: *Numerical Simulation of Mechatronic Sensors and Actuators.* Springer, 2nd edition, 2007.

[7] Rifai, S. M., Johan, Z., Wang, W.-P., Grisval, J.-P., Hughes, T. J. R. & Ferencz, R. M.: *Multiphysics simulation of flow-induced vibrations and aeroelasticity on parallel computing platforms.* Computer Methods in Applied Mechanics and Engineering, vol. 174, pp. 393–417, 1998.